6166 *Macromolecules* **2009**, *42*, 6166–6174
DOI: 10.1021/ma900954c

Macromolecules
ARTICLE

A Route for the Thermodynamic Description of Strain-Induced Crystallization in Sulfur-Cured Natural Rubber

Masatoshi Tosaka*

Institute for Chemical Research, Kyoto University, Uji, Kyoto 611-0011, Japan

Received May 1, 2009; Revised Manuscript Received June 23, 2009

ABSTRACT: There has been an implicit problem that, in the previous treatments, some behaviors of strain-induced crystallization in cross-linked natural rubber (NR) and synthetic *cis*-1,4-polyisoprene (IR) were inconsistent with the predictions on the basis of the statistical theory of rubber elasticity. This problem was found to have come from disregard for the existence of the fluid-like network-chain component. In this study, the rubber sample is assumed to be composed of the elastically effective as well as the fluid-like components and their physical quantities are separately considered. The corresponding mechanical model can explain the features of strain-induced crystallization successfully. The mechanical model is assessed using the tensile stress−strain behavior of NR and IR samples at very fast deformation rate.

Introduction

The plant-derived natural rubber (NR) is an indispensable material for many industrial and household applications, especially for heavy-duty use.[1] The good performance of NR products has been thought to originate from the ability to crystallize immediately by extension. Compared to the synthetic counterpart (*cis*-1,4-polyisoprene rubber; IR), the enhancement of tensile modulus along with the superior stress at break and tear strength under fast deformation should be related to the formation of strain-induced crystals.[2−4] Thus strain-induced crystallization of NR has been attracting the interest of many researchers.[5]

Although strain-induced crystallization of NR has been extensively studied even before the advent of macromolecular physics,[6] there are still some unsolved basic issues in this field, which are summarized in a recent review article.[5] From the industrial viewpoint, we still do not know much how to improve the mechanical properties of rubber materials through the use of the strain-induced crystallization behavior. For example, in the case of thermoplastic semicrystalline polymers such as polyethylene or polypropylene, mechanical properties can be improved by mixing with nucleating agents that enhance crystallization. On the other hand, in the case of vulcanized NR and IR, stearic acid (nucleating agent for NR[7−11]) does not enhance strain-induced crystallization.[12] Thus we still cannot develop a rubber material that can perfectly substitute for NR.

The key issue is that we are still exploring a framework to deal with strain-induced crystallization in cross-linked rubber using thermodynamic formulations. Because such a framework has not been established, we still cannot explain the experimental features nor consider quantitatively the effects of extension ratio, tensile stress, ambient temperature, etc., on strain-induced crystallization. This has been an implicit disadvantage in the rubber industry because the material design has to rely on experience and instinct of experts.

As strain-induced crystallization is a phase transition, undoubtedly, thermodynamics on deformation of network polymer concerns. In the thermodynamics, state variables are defined under the equilibrium condition. If we assume the equilibrium also under deformed state, the state variables are still defined. As long as the degree of deformation is unchanged, the relationship between the state variables, namely the state equations, should hold. Even in the discussion of nonequilibrium dynamics, we can extend the usage of the state variables and state equations to the deformed state. In this way, we should be able to handle not only strain-induced crystallization but also the rubber elasticity in terms of thermodynamics. Indeed, we know that the statistical theory of rubber elasticity[13] has successfully established thermodynamic formulations for deformation and swelling behavior of amorphous network polymer. In the statistical theory, fluctuation of the molecular network structure is statistically averaged over the system, and the physical quantities are represented by the average values. The advantage of the statistical theory is the convenience that we can reasonably explain experimental results using a small number of parameters. Thus usage of the statistical theory is not limited to the field of network polymers but applied also to rheology of linear chain polymers (e.g., to the calculation of entanglement density in the polymer melt). As the statistical theory is widely accepted in this way, it is a natural consequence to apply thermodynamic descriptions in this theory to strain-induced crystallization. The prediction in the past about the occurrence of strain-induced crystallization on the basis of the statistical theory was, however, inconsistent with the experimental results as shown shortly. Despite rubber elasticity and strain-induced crystallization are both related to thermodynamics on the deformation of network polymer, why the prediction for the latter was not successful?

The author found that the recognition of the existence of a fluid-like (elastically ineffective) component in the cross-linked rubber leads to the construction of a framework for thermodynamic description of strain-induced crystallization. In the beginning of this article, we discuss peculiar experimental features of strain-induced crystallization. Then we propose a route to deal with strain-induced crystallization using the formulations in the statistical theory.

Experimental Features of Strain-Induced Crystallization. In a variety of papers, the following features (hereafter, they are referred to as the first, second and third features) on strain-induced crystallization of cross-linked NR have been reported.

*Corresponding author. Telephone: +81-774-38-3062. Fax: +81-774-38-3069. E-mail: tosaka@scl.kyoto-u.ac.jp.

 Published on Web 07/10/2009

(*1*). *Coexistence of Extremely Different Network Chains*. In wide-angle X-ray diffraction (WAXD) patterns of a NR sample during the tensile extension, highly oriented crystalline reflections appear without preceding localization of halo intensity. On the other hand, isotropic amorphous halo remains even when the sample is highly stretched. As a result, the oriented crystalline reflections and the isotropic halo are observed simultaneously.[14−20] This feature directly indicates the coexistence of highly stretched molecular chains and randomly coiled ones. Quantitative analysis of the WAXD patterns has led to a conclusion that majority of chains are in the state of isotropic coils even in the highly stretched sample; only a few percent of the amorphous chains are oriented.[17,18] Computer simulation of deformed polymer network[21,22] also indicated that tensile stress is localized on a small number of highly stretched paths, while the other chains are considerably relaxed.

In another case, when the stretched sample was cooled or stored for a long time, formation of two or more types of morphologically different crystals was reported.[23−25] The morphological difference may be due to the coexistence of strained and relaxed network chains. This view is further supported by observation of internal structure of stretched samples that revealed formation of fibrillar texture.[26−30]

These experimental results suggest dichotomization of network chains into highly oriented and unoriented components. The phase behavior of these extremely different network chains should be apart from that of their statistical average.

(*2*). *Incipient Strain of Crystallization*. There have been several reports that the extension ratio at the onset of crystallization, α_i, during the stretching process was almost independent of network-chain density.[19,20,31−34] NR samples filled with carbon black also presented the α_i values which were independent of network-chain density, after correction of the extension ratio to the effective one for the deformable rubber portion.[32]

These experimental results have been inconsistent with the predictions in the previous treatments on the basis of the statistical theory. When uniaxial extension of cross-linked rubber is considered, the nominal stress at an extension ratio α, namely $\sigma(\alpha)$, is explained as,[13,35]

$$\sigma(\alpha) = \frac{\mathrm{d}W(\alpha)}{\mathrm{d}\alpha} \tag{1}$$

$$W(\alpha) = U(\alpha) - TS(\alpha) \tag{2}$$

where $W(\alpha)$ is so-called the strain-energy function, $U(\alpha)$ the internal energy, T the absolute temperature, and $S(\alpha)$ the entropy. Because the contribution of $U(\alpha)$ is very small for the rubber elasticity, combination of eqs 1 and 2 yields

$$\sigma(\alpha) \approx \frac{-T\,\mathrm{d}S(\alpha)}{\mathrm{d}\alpha} \tag{3}$$

Then the entropy change of deformation from $\alpha = 1$ to $\alpha = \alpha_1$, namely ΔS_{def}, is related to the tensile stress as,

$$\Delta S_{\mathrm{def}} \approx -\frac{1}{T}\int_1^{\alpha_1} \sigma(\alpha)\,\mathrm{d}\alpha \tag{4}$$

Equation 4 indicates that ΔS_{def} is larger for the "harder" sample having the higher network-chain density. Now, strain-induced crystallization is an entropy-driven phase transition which should be related to ΔS_{def}. Thus theoretical works applying the statistical theory to strain-induced crystallization[36,37] have predicted that α_i should depend on network-chain density. For example, the basic idea presented by Yamamoto and White[36] was as follows. "When the amorphous sample is expanded, the network chains become oriented in the stretching direction and their end-to-end distances are increased. The orientation, stretching, and thus partial ordering of the polymer chains decrease the configurational entropy of the sample by an amount ΔS_{def} and thus decrease the entropy change of fusion." By applying thermodynamic formula for equilibrium, they assumed that the melting temperature at an extension ratio α, namely $T_{\mathrm{m}}(\alpha)$, is given as,

$$T_{\mathrm{m}}(\alpha) = \frac{\Delta H(\alpha)}{\Delta S(\alpha)} \tag{5}$$

where $\Delta H(\alpha)$ is the heat of fusion at the extension ratio α. Due to the decreased entropy change of fusion, the melting temperature at $\alpha = \alpha_1$ will be elevated by an amount

$$T_{\mathrm{m}}(\alpha_1) - T_{\mathrm{m}}(1) = \frac{\Delta H(\alpha_1)}{\Delta S(\alpha_1)} - \frac{\Delta H(1)}{\Delta S(1)} \tag{6}$$

As the heat of fusion is thought to be independent of the deformation ($\Delta H(\alpha) = \Delta H(1)$), eq 6 will be rewritten as

$$\frac{1}{T_{\mathrm{m}}(\alpha_1)} = \frac{1}{T_{\mathrm{m}}(1)} + \frac{\Delta S_{\mathrm{def}}}{\Delta H(1)} \tag{7}$$

When $T_{\mathrm{m}}(\alpha_1)$ exceeds the ambient temperature and attains sufficient supercooling, strain-induced crystallization will take place. As the above equations show, the tensile stress due to rubber elasticity and occurrence of strain-induced crystallization have the same origin, namely the entropy change of deformation, ΔS_{def}. Analytical formulation of ΔS_{def} (eq 4), and hence the explicit form of eq 7, depends on the description of the strain-energy function. For example, the simplest expression of ΔS_{def} assuming the Gaussian chains is[13]

$$\Delta S_{\mathrm{def}} = -\frac{1}{2}\nu k\left(\alpha^2 + \frac{2}{\alpha} - 3\right) \tag{8}$$

where ν is network-chain density and k is the Boltzmann constant. Combination of eqs 7 and 8 yields

$$\frac{1}{T_{\mathrm{m}}(\alpha_1)} = \frac{1}{T_{\mathrm{m}}(1)} - \frac{\nu k\left({\alpha_1}^2 + \frac{2}{\alpha_1} - 3\right)}{2\Delta H(1)} \tag{9}$$

This is a somewhat simplified expression for the convenience of the readers. As a result of more rigorous treatment, for example, Flory proposed the next formulation[37]

$$\frac{1}{T_{\mathrm{m}}(\alpha_1)} = \frac{1}{T_{\mathrm{m}}(1)} - \frac{R}{\Delta H(1)}\left[\left(\frac{6m_0\nu}{\pi\rho}\right)^{1/2}\alpha_1 - \frac{m_0\nu}{\rho}\left(\frac{{\alpha_1}^2}{2} + \frac{1}{\alpha_1}\right)\right] \tag{10}$$

where R is the gas constant, m_0 the mass of statistical segments, and ρ the specific gravity. Flory defined $T_{\mathrm{m}}(\alpha_1)$ in eq 10 as "incipient crystallization temperature", which should be practically regarded as the melting temperature.

Equations 9 and 10 should be essentially correct, because they can reasonably explain the difference between NR and IR. IR samples required the larger α_i value than NR ones.[19] According to eqs 9 and 10, this is a consequence of the lower $T_{\mathrm{m}}(1)$ of IR. The lower melting temperature of IR, not only in unstretched but also in stretched states, has been reported by Gent et al.[2] and Trabelsi et al.[38] Because melting temperature must be elevated above ambient temperature from the lower $T_{\mathrm{m}}(1)$ for the onset of strain-induced crystallization, the larger extension was required for IR. The lower $T_{\mathrm{m}}(1)$ of IR is due to the lower regularity in the main-chain structure.[39,40]

On the other hand, both the eqs 9 and 10 predict that the samples with the higher network-chain density can attain the same incipient crystallization temperature at lower extension ratio, leading to the smaller α_i. As has been already mentioned, however, the experimental works reported that α_i was almost independent of network-chain density. More detailed discussion on this issue has been presented before.[5] (Recently, a case that α_i depended on network-chain density was reported for a series of samples using a different cross-linking agent.[41,42] We will discuss this exceptional case later.)

Additionally, we have obtained the following peculiar experimental results.

(*3*). *Stress Relaxation Due to Strain-Induced Crystallization*. When a sample is quickly extended and kept at a relatively high constant strain, strain-induced crystallization progresses with time. In our experiments, as shown in Figure 1,[4] the rate of strain-induced crystallization depended on network-chain density; the sample with the higher network-chain density crystallized the faster during the initial stage. Figure 1 also indicates that NR crystallized faster than IR.

In this type of experiment, strain-induced crystallization induces stress relaxation because the molecular chains in the crystals adopt the extended conformation aligned in the stretching direction.[20,37,38,43−47] Accordingly, the samples exhibit the maximum stress at the moment when the extension is stopped. Here, the stress values normalized by the maximum stress (hereafter, we refer to it as "normalized stress") were evaluated to compare the degree of stress relaxation among the samples having different values of modulus (Figure 2). The relaxation rates of the normalized stress for NR samples were faster than those of IR ones, reflecting the rate of strain-induced crystallization. However, the difference in network-chain density hardly affected the relaxation rate of the normalized stress, regardless to the different rate of strain-induced crystallization (Figure 1).[4,48]

This feature also leads to a contradictory situation. As mentioned above, the molecular chains in the crystals stabilize in the extended chain conformation and only the amorphous chains exhibit rubber elasticity. Then the tensile stress should change from the initial value with the progress of crystallization as illustrated in Figure 3. The sample with the faster rate of strain-induced crystallization is expected to show the faster relaxation in the normalized stress. This is true if we compare the NR and IR samples. The solid and broken lines in Figure 3b correspond to NR and IR, respectively. However, if we compare the samples with different network-chain densities, this expectation is inconsistent with the experimental results (see Figure 2). In order to overcome this problem, in the previous articles,[5,48] stretched chains responsible for strain-induced crystallization were separately considered from the relaxed chins. In the following part of this article, this idea is extended to explain the features of strain-induced crystallization in the unified viewpoint.

Mechanical Model to Deal with Strain-Induced Crystallization in Terms of Thermodynamics. As mentioned above, application of the statistical theory was not successful for the explanation of the second feature of strain-induced crystallization. To find the origin of this problem, the author focused attention on the first feature of strain-induced crystallization.

According to the conservation of the isotropic halo regardless of deformation, a considerable amount of amorphous chains should be relaxed immediately after (or during) deformation, that is to say, they are acting like a fluid mass. Consequently, these chains should be excluded from the mass fraction that is responsible for rubber elasticity and

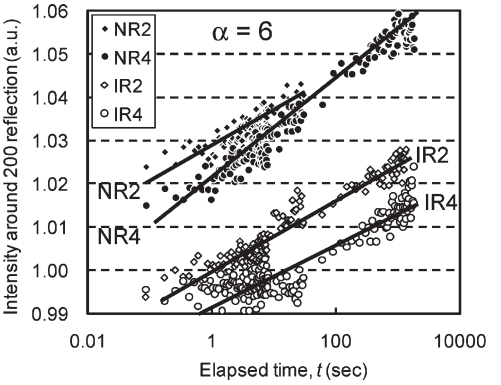

Figure 1. Time-dependent change of integrated intensity around the 200 reflection in the WAXD patterns of the NR and IR samples. The larger intensity indicates the more development of strain-induced crystallization. The solid lines are guides for eyes. The samples were quickly extended up to 6 times the original length and kept at the length. The elapsed time indicates the length from the completion of the extension. The characteristics of NR and IR samples are shown in Table 1. The horizontal axis is indicated by the logarithmic scale. The original data and the details of the experimental procedures have been reported in ref 4.

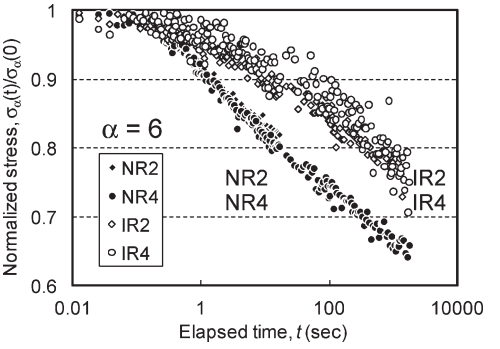

Figure 2. Time-dependent change of normalized tensile stress. The tensile data were collected simultaneously with the WAXD patterns used in Figure 1. The difference in network-chain density did not appreciably affect the rate of relaxation, while the difference between NR and IR samples was apparent. The characteristics of NR and IR samples are shown in Table 1. The horizontal axis is indicated by the logarithmic scale. The original data and the detail of experimental procedure have been reported in ref 4.

occurrence of strain-induced crystallization. Thus the author supposed that the network chains in cross-linked rubber should be regarded as a combination of the elastically effective and the fluid-like components when strain-induced crystallization is dealt with. Since these two components are in quite different states, their physical quantities are considered separately.

It is noteworthy that the similar idea assuming the two types of components in the network polymer has been proposed by James and Guth[35] when their rubber elasticity theory was constructed. On the basis of rigorous mathematical treatment, they presented that the complicated network structure of inhomogeneous rubber can be replaced by equivalent linear chains responsible for the rubber elasticity and elastically ineffective chains acting like an incompressible fluid. Then the average elastic response of this model was calculated. In the case of Gaussian chain statics, even without assuming the uniformity of the network-chain length and the affine deformation, they derived essentially the same formulations for rubber elasticity as the ones based on the affine deformation of a uniform network structure. Accordingly, their work has been regarded as a rigorous proof of the

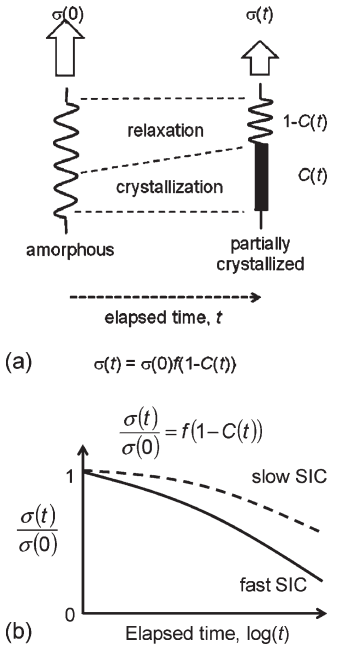

Figure 3. Schematic representation of stress relaxation due to strain-induced crystallization. The left side of part (a) illustrates the amorphous rubber sample just after the quick extension. The stress at this moment is $\sigma(0)$. With the elapsed time t, strain-induced crystallization progresses. Parts of molecular chains in the crystals occupying $C(t)$ of fraction stabilize in the extended chain conformation. As a result, strain in the other parts of molecular chains in the amorphous phase is reduced. This process is indicated as "relaxation" in part a. At the same time, the fraction of amorphous chains decreases to $1-C(t)$. Thus the tensile stress $\sigma(t)$ changes from the initial value, $\sigma(0)$, as a function of the amorphous fraction. That is to say, $\sigma(t)=\sigma(0)f(1-C(t))$, and accordingly, $\sigma(t)/\sigma(0) = f(1 - C(t))$; the plot $\sigma(t)/\sigma(0)$ against elapsed time as in part b should be related to the fraction of amorphous phase, $1 - C(t)$.

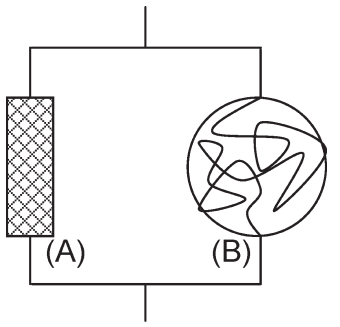

Figure 4. Mechanical model representing the coexistence of two types of network components. Component A is responsible for rubber elasticity, while component B is elastically ineffective, acting like a fluid mass. In this figure, the former is illustrated as a rubber band, and the latter as a flexible bag filled with a viscoelastic liquid.

validity of some statistical assumptions in the theory of rubber elasticity.[13] Now, in dealing with rubber elasticity or swelling behavior, only the averaged physical quantities of the two components were sufficient, because they are macroscopic phenomena. For the description of strain-induced crystallization of cross-linked NR, on the other hand, we must reconsider the primitive network model by James and Guth. As crystallization is a phenomenon in the nanoscopic scale, its behavior may be influenced by the local environment around the elastically effective chains. In order to consider the response of the two types of network chains separately, a mechanical model as in Figure 4 is proposed.

Table 1. Recipes and Cure Conditions of Vulcanized Rubber Samples

sample code	rubber[a] (part)	stearic acid (part)	active ZnO (part)	CBS[b] (part)	sulfur (part)	curing time (min)	network chain density, $\bar{\nu} \times 10^4$ (mol/cm^3)
NR1	100	2	1	3	4.5	10	2.12
NR2	100	2	1	2	3	12	1.78
NR3	100	2	1	1.5	2.25	12	1.46
NR4	100	2	1	1	1.5	14	1.31
NR5	100	2	1	0.75	1.125	17	1.01
IR1	100	2	1	3	4.5	17	1.99
IR2	100	2	1	2	3	17	1.66
IR3	100	2	1	1.5	2.25	21	1.36
IR4	100	2	1	1	1.5	25	1.29
IR5	100	2	1	0.75	1.125	30	1.03

[a] NR is RSS No. 1 from Malaysia and IR is IR2200 from JSR. [b] *N*-Cyclohexyl-2-benzothiazole sulfenamide, curing temperature with sulfur 140 °C.

In Figure 4, component A represents the elastically effective network chains. This component itself is dealt with by the conventional formulations in the statistical theory.[13] A hypothetical network-chain density value, ν_0, is attributed to this component. On the other hand, component B represents the elastically ineffective chains, acting like a fluid. Tentatively, a negligibly small network-chain density value, ν_1, is attributed to this component, because there should be a finite number of chains in the unit mass. The mass fractions of components A and B are defined to be ϕ and $(1 - \phi)$, respectively. The apparent values of network-chain density (e.g., in Table 1) and crystallinity measured by the experiments are regarded to reflect the averages over the components A and B. For example, the average (apparent) network-chain density is written as,

$$\bar{\nu} = \phi\nu_0 + (1-\phi)\nu_1 \approx \phi\nu_0 \qquad (11)$$

In this equation and the following discussion, we assume that additivity relationship holds for this system. This relationship was also implicitly assumed in the work by James and Guth.[35]

Let us apply the model in Figure 4 to the interpretation of the experimental features of strain-induced crystallization. We remember that eqs 9 and 10 predict that the incipient extension ratio of crystallization, α_i, will depend on network-chain density. In the present model, we consider only component A as the crystallizing entity, and accordingly, the network-chain density value substituted in these equations should be ν_0, instead of the apparent value, $\bar{\nu}$. The common α_i value in the experiment (the second feature of strain-induced crystallization) implies, in the reverse way, that the series of samples happened to have had almost the same ν_0 values. (A recent study[49] gave a structural basis for this interpretation, as discussed later.) When we adopt this interpretation, the second feature of strain-induced crystallization and formulations of the statistical theory such as eqs 9 and 10 can be compatible.

Under the assumption that the series of samples have a common ν_0 value, eq 11 implies that the apparent $\bar{\nu}$ values reflect the volume fraction, ϕ, of component A in Figure 4. Then the third feature of strain-induced crystallization is also successfully explained as follows. In the experimental condition in question (for Figures 1 and 2),[4,48] the rubber sample is quickly extended to a sufficiently high extension ratio and kept at the constant length. Crystallinity in this sample increases with elapsed time, t. As component A is the crystallizing entity, its crystallinity should change as a function of t and ν_0 in the similar way as in Figure 3a. That is to say, the crystallinity of component A is expressed as $C_{0\alpha}(t, \nu_0)$. Then, the crystallinity of the entire sample (namely, apparent

crystallinity), $C_\alpha(t, \overline{\nu})$, is obtained by multiplying $C_{0\alpha}(t, \nu_0)$ with the volume fraction of the component A:

$$C_\alpha(t, \overline{\nu}) = \phi C_{0\alpha}(t, \nu) \tag{12}$$

At a certain elapsed time, the apparent crystallinity (and the intensity of crystalline reflection) shall be higher for the sample with the higher $\overline{\nu}$ because of the larger ϕ (eq 11). This prediction is consistent with the feature in Figure 1 when we compare NR2 and NR4 (or IR2 and IR4). The difference between NR and IR samples (Figure 1) is attributed to difference in $C_{0\alpha}(t, \nu_0)$ (or in the rate of crystallization, $(\partial/\partial t)C_{0\alpha}(t, \nu_0)$).

With the progress of strain-induced crystallization, tensile stress, σ, to hold the sample at the fixed extension ratio also changes, as mentioned above. For the unit cross-sectional area of component A, the tensile stress is assumed as a function of crystallinity, and accordingly, of t and ν_0. In the same way as above, we can express the tensile stress for component A as $\sigma_{0\alpha}(t, \nu_0)$. Considering the volume fraction of component A, the tensile stress for the entire sample is

$$\sigma_\alpha(t, \overline{\nu}) = \phi\sigma_{0\alpha}(t, \nu_0) \tag{13}$$

In Figure 2,[4,48] the stress value normalized by the initial one (at $t = 0$), namely $\sigma_\alpha(t, \overline{\nu})/\sigma_\alpha(0, \overline{\nu})$, was examined. Using eq 13, this value is rewritten as,

$$\frac{\sigma_\alpha(t, \overline{\nu})}{\sigma_\alpha(0, \overline{\nu})} = \frac{\phi\sigma_{0\alpha}(t, \nu_0)}{\phi\sigma_{0\alpha}(0, \nu_0)} = \frac{\sigma_{0\alpha}(t, \nu_0)}{\sigma_{0\alpha}(0, \nu_0)} \tag{14}$$

Because ν_0 is assumed to be common for the series of samples, the right side of eq 14 is also common among them. Then the plots of $\sigma_\alpha(t, \overline{\nu})/\sigma_\alpha(0, \overline{\nu})$ vs t should be common for the series of samples, that is to say, the plots should overlap with each other as in Figure 2. The third feature of strain-induced crystallization for each series of NR and IR samples with different $\overline{\nu}$ can be thus reproduced. (Note that $\sigma_{0\alpha}(t, \nu_0)$'s for NR and IR are different, reflecting the different rate of strain-induced crystallization.)

In this way, simply by assuming the coexistence of the fluid-like component with the elastically effective one that can be dealt with by the conventional formulations in the statistical theory, the behavior of strain-induced crystallization in cross-linked NR can be explained consistently with the expectedly correct theories.[36,37] The advantage of the above treatment is that the existing thermodynamic descriptions of the statistical theory can be applied to strain-induced crystallization with minimum modification. The increase in the number of parameters is minimized, compared to complicated treatment in the earlier works, e.g., by considering the distribution of network-chain lengths.[28]

Assessment of the Two-Component Model. In the above discussion, the series of samples were assumed to have had the common ν_0 value. This assumption appeared to be, at first, questionable even for the author. In order to access the validity of this assumption along with the two-component model, the stress−strain behaviors of the series of samples were examined. Since Figure 4 is a mechanical model, the stress−strain relationship may be used for the assessment.

We tentatively describe the nonequilibrium tensile stress for unit mass of component A as a function of extension ratio and network-chain density, namely $\sigma_0(\alpha, \nu_0)$. By assuming the mechanical model in Figure 4, the nonequilibrium tensile stress for the entire rubber sample is expressed as

$$\sigma(\alpha, \overline{\nu}) = \phi\sigma_0(\alpha, \nu_0) + (1 - \phi)\sigma_\nu \tag{15-1}$$

$$\approx \phi\sigma_0(\alpha, \nu_0) \tag{15-2}$$

where σ_ν represents viscoelastic force which is introduced to consider the contribution of component B; σ_ν is practically the force for the deformation of the liquid-like polymer. When the last term in eq 15-1 is comparatively small, the approximation in eq 15-2 would hold. In the reverse way, the approximation to eq 15-2 requires the first term in the right side of eq 15-1 to be large enough for all the samples. Such a situation will be achieved at a sufficiently high strain. If the strain is too high, however, formation of strain-induced crystals can modify the network structure itself. Therefore, we assume an extension ratio value α_n which is large enough but still below the incipient extension ratio of crystallization, α_i. At this extension ratio α_n, according to eq 15-2,

$$\phi \approx \frac{\sigma(\alpha_n, \overline{\nu})}{\sigma_0(\alpha_n, \nu_0)} \tag{16}$$

and substitution of eq 16 into eq 15-2 yields,

$$\frac{\sigma(\alpha, \overline{\nu})}{\sigma(\alpha_n, \overline{\nu})} \approx \frac{\sigma_0(\alpha, \nu_0)}{\sigma_0(\alpha_n, \nu_0)} \tag{17}$$

The left side of eq 17 corresponds to the observed stress after normalization by the stress value at extension ratio α_n, while the right side should be common for the series of samples. This equation suggests that the stress−strain curves for the series of samples become identical after the normalization by $\sigma(\alpha_n, \overline{\nu})$. If this feature appears, the assumption and the two-component model should be reasonable.

Before proceeding to the Experimental Section, the experimental condition for the above assessment method must be noted. The tensile stress at temperature T is expressed as;[13]

$$\sigma = \nu kT\left(\alpha - \frac{1}{\alpha^2}\right) \tag{18}$$

when we assume the equilibrium Gaussian chain statistics. This equation predicts that the stress−strain curves will be identical after the normalization of eq 17, regardless to the validity of the current treatment. In order to avoid this problem, we stretch the rubber sample at a very fast deformation rate so that the tensile behavior departs from the equilibrium Gaussian one.[33]

Hereafter, we examine our stress−strain relationship on the basis of the above discussion.

Experimental Section

The experimental procedure was essentially the same as the one in our previous paper.[4] Vulcanized NR (RSS No. 1) and IR (IR2200, JSR) samples were prepared according to the recipes and cure conditions in Table 1. The preparation and characterization procedures of the vulcanized rubber sheets (1 mm thick) have been reported in the earlier works.[19,20] Ring-shaped specimens[4] were die-cut from the sheets. The inner and outer diameters of the specimens were 11.7 and 13.7 mm, respectively (ca. 40 mm circumference). The ambient temperature was controlled to be 25 °C. The specimen was stretched up to 7 times the original length. The maximum speed of the custom-made tensile tester (500 mm/min) was used. Because initial length of the ring-shaped specimen corresponds to the half of its circumference, the deformation rate was 25 min^{-1} when the entire specimen deformed uniformly. By analyzing the WAXD data in our previous studies,[4,48] we confirmed that α_i values of NR and IR samples have been estimated to be ca. 4.5 and 6, respectively, in this experimental condition. (The higher stretching speed compared to the experiments in refs 19 and 20 was employed, and accordingly, the α_i values were shifted.)

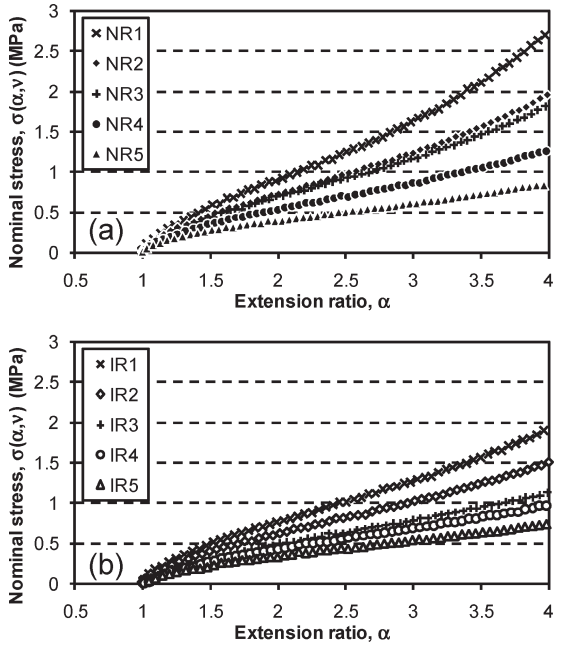

Figure 5. Part of the stress−strain curves for the NR (a) and IR (b) samples.

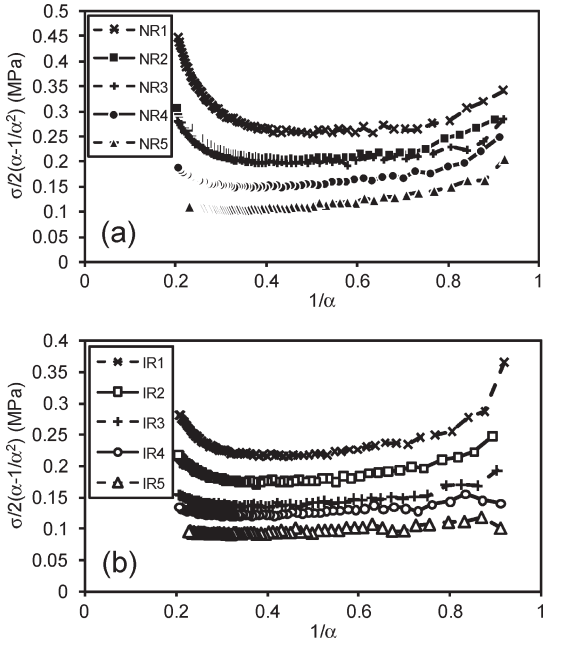

Figure 6. Mooney−Rivlin plot of the stress−strain data for the NR (a) and IR (b) samples.

Results and Discussion

Figure 5 shows a part of the stress−strain curves of NR and IR samples. The sample with the higher $\bar{\nu}$ value exhibited the higher stress at the same extension ratio. Furthermore, if we compare the samples having the similar $\bar{\nu}$ values (e.g., NR3 and IR2), the stress values of NR samples are mostly higher than those of the IR ones (though the NR3 has a slightly lower $\bar{\nu}$ value than IR2). This is not due to the higher crystallinity of NR for the region presented in this figure. Even before the occurrence of strain-induced crystallization at a smaller strain, NR samples showed the higher stress. It is noted that the $\bar{\nu}$ values were estimated from the initial slopes of σ vs $(\alpha - \alpha^{-2})$ plots in other tensile experiments[13,20] adopting a slower deformation rate. The larger $\bar{\nu}$ value implies that the tensile modulus was higher for, e.g., IR2 than NR3 when the slower deformation rate was adopted. The inversion of the tensile stress between IR2 and NR3 is obviously brought about by the faster deformation rate.

Figure 6 shows the Mooney−Rivlin plot[13] of the stress−strain data for the NR and IR samples. It is known that the equilibrium behavior of the Gaussian chains presents linear lines in this type of plot. In the classic studies on cross-linked NR, the experimental data were indeed linear when $1/\alpha$ is relatively high, though they deviated from the linearity due to finite extensibility of network-chains as $1/\alpha$ becomes small.[13] In Figure 6, on the other hand, the plots are nonlinear even when $1/\alpha$ is relatively large. These results indicate that the tensile behaviors of the samples at the fast deformation rate deviated from the equilibrium one. That is to say, the approximation of eq 18 is not applicable to the stress−strain data in Figure 5.

The stress−strain data were normalized by the stress values at $\alpha_n = 3$. This α_n value was selected because it was sufficiently smaller than α_i, even when the deformation rate was much slower.[19,20] Figure 7 shows the normalized stress−strain curves and Figure 8 is the enlargement of Figure 7 in the range of $\alpha < 3$. In these figures, NR and IR samples show different feature when the extension ratio is lower than 3. As expected from eq 17, the stress−strain curves of all IR samples almost overlap with each other up to $\alpha \approx 3$ (Figure 8b). Above this extension ratio, the stress for the sample with the higher $\bar{\nu}$ tends to upturn the more. On the other hand, in the case of NR, the samples with the lower $\bar{\nu}$

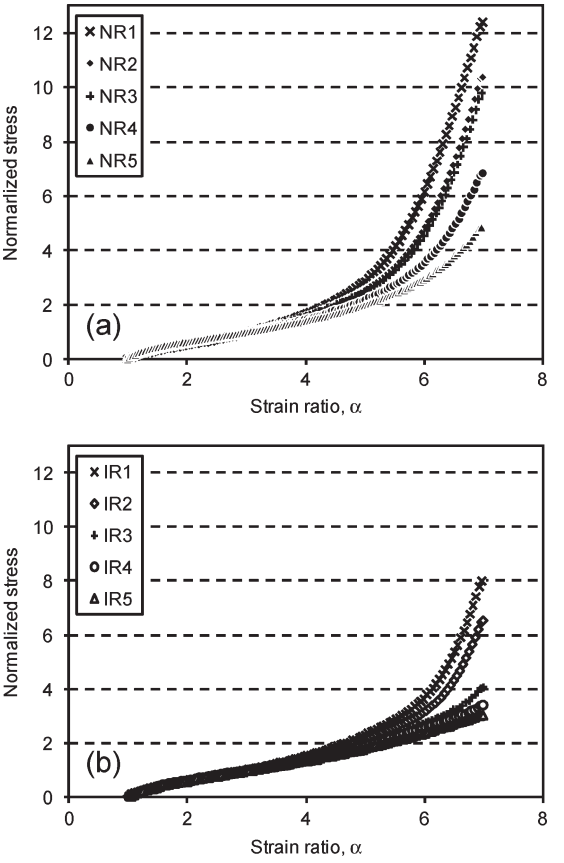

Figure 7. Normalized stress−strain curves for the NR (a) and IR (b) samples.

show the higher normalized stress even when the extension ratio is lower than 3 (Figure 8a). The results for the IR samples in the lower range of extension ratio are directly consistent with the assumption that these samples had the common ν_0 value. Accordingly, the treatment using the two-component model in Figure 4 should be reasonable in dealing with strain-induced

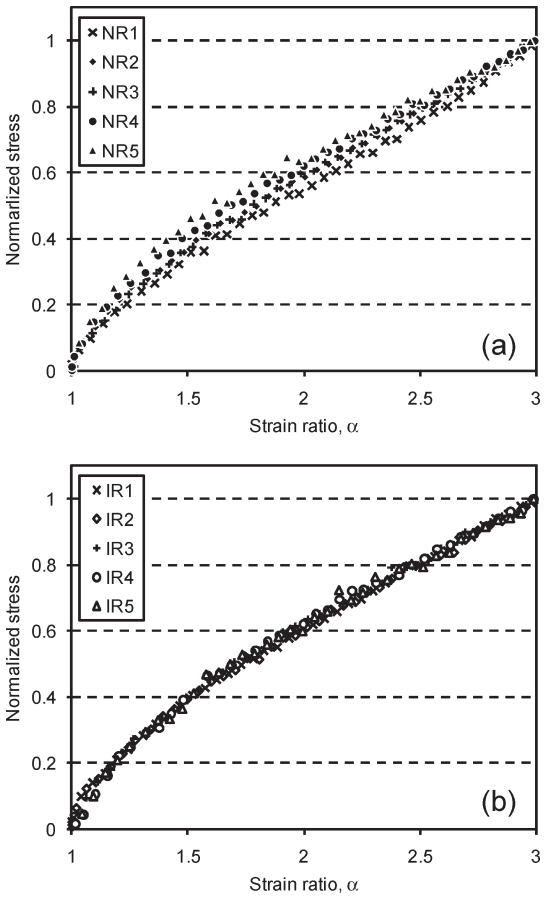

Figure 8. Enlargement of the normalized stress−strain curves for the NR (a) and IR (b) samples in the range of small strain.

crystallization in terms of thermodynamics. For the further justification of the current treatment, the other features in Figures 7 and 8 should be discussed.

In the case of NR samples, even in the range of the low extension ratio, the normalized stress−strain curves were somewhat different from each other (Figure 8a). This is seemingly inconsistent with the expectation from eq 17. However, the discrepancy is attributed to the viscoelastic contribution of the fluid-like component (see eq 15-1). It is known that the nonrubber contents in NR have significant effects on the physical properties. For example, temporal aggregate structures of proteins or phospholipids greatly enhance the green strength (namely, the tensile strength of unvulcanized rubber) of NR compared to IR.[40,50−53] That is to say, the effects of nonrubber contents on mechanical properties are more apparent in the states of low- or noncross-linking. As a result of the existence of the nonrubber contents, the viscoelastic contribution of the fluid-like component B may have been enhanced only for NR samples. The trend that the NR samples with the smaller $\bar{\nu}$ show the larger normalized stress (Figure 8a) is related to the larger fraction of the fluid-like component. The larger stress of NR compared to IR even before the onset of strain-induced crystallization (Figure 5) is also explained by considering the effect of the nonrubber contents; inclusion of the nonrubber contents should tend to increase the modulus under the condition of the fast deformation rate.

The other point to be considered is the tensile behavior in the high strain region ($\alpha > 3$). Even after the normalization, the stress−strain curves were different from sample to sample in this region (Figure 7). However, the discrepancy in this region is not due to a problem of the two-component model. In the first place, $\sigma(\alpha, \nu)$ is an oversimplified expression for the tensile behavior of cross-linked rubber. For the exact expression of the tensile behavior up to the high extension ratio, we have to apply alternative form of the strain-energy function (see eq 1) using an increased number of parameters.[54,55] That is to say, the tensile behavior in the high strain region is out of the applicability of the simple expressions in eqs 15 to 17, and accordingly, has nothing to do with the assessment in our treatment.

In this way, for the cross-linked samples, the simple mechanical model in Figure 4 could explain not only the features of strain-induced crystallization but also the difference in tensile behaviors between NR and IR in the region of low extension ratio with the minimum increase in the number of parameters.

A recent study[49] disclosed that the α_i values for the vulcanized NR samples were related to the composition of the stearic acid and/or active zinc oxide. When cross-linked rubber samples were swollen, the inhomogeneity was represented by the combination of swollen gel and solid-like domains. The sample that showed the same α_i value had the same mesh size for the swollen gel, which was determined by the composition of these ingredients. The fixed composition of these ingredients in the series of samples indicated in Table 1 should have led to the same α_i value, and hence to the common ν_0 value. In another case, α_i depended on the $\bar{\nu}$ values,[41,42] that is to say, the ν_0 values were different from sample to sample, due to the absence of stearic acid and active zinc oxide; the samples were cross-linked using dicumyl peroxide. As shown in these studies, certain features of the inhomogeneous network structure determine the ν_0 value for the description of strain-induced crystallization behavior. The different α_i values reported by other groups[33,34] should result from the different recipes. It is noted that the mesh size of the swollen gel is not directly converted to the ν_0 value because these values are attributed to totally different models. Finding the connection between these two parameters is our future task.

Tangible values of ϕ and ν_0 would be of interest to the readers. There are some ways to estimate them. For example, James and Guth[35] have suggested the formulation to estimate the fraction, ϕ, of elastically effective component from the stress−strain data. Unfortunately, their formulation did not give reliable values for the samples in this study. Alternatively, the author roughly estimated the ν_0 value from the effective melting temperature (namely, melting temperature of polymer crystals of finite size) of the unstretched NR samples and the extension ratio at which the strain-induced crystals disappear, namely α_e, during the retraction process. In general, the effective melting temperature of polymer depends on the corresponding crystallization temperature. In the case of strain-induced crystallization, however, direct measurement of the effective melting temperature is very difficult. The effective melting temperature for the estimation of the ν_0 value was, therefore, assumed by considering lamellar crystals grown rapidly. According to the former studies,[2,56,57] measured melting temperature of NR distributes from ca. −2 to +18 °C. (Melting temperature of NR does not depend on network-chain density.[56]) When crystallization temperature between −25 and −10 °C, at which NR crystallizes relatively fast, was selected, then the measured melting temperature was 0 ± 2 °C. This value is consistent with the one expected from the polymer crystallization theory.[58] Melting temperature, T_m, of polymer crystals with lamellar thickness l is

$$T_m < T_m^0 \left(1 - \frac{2\sigma_e}{l\Delta H}\right) \tag{19}$$

where T_m^0 is the equilibrium melting temperature and σ_e is the fold-surface free energy of the polymer under consideration. T_m^0 of *cis*-1,4-polyisoprene is reported to be 35 °C and ΔH has been estimated to be 61 J/cm^3.[59,60] Two values of σ_e have been reported for morphologically different crystals of NR as a result of different direction of chain folding: For the α crystal, $\sigma_e = 0.0239$

J/m^2 and for the β crystal, $\sigma_e = 0.0503\ J/m^2$.[61] Because the strain-induced crystals may have irregular chain folding, the averaged T_m value for the α and β crystals was adopted. If we assume $l = 10$ to 12 nm, in which range the lamellar thickness is a typical value of lamellar polymer crystals, T_m was estimated to be 0 ± 3 °C from eq 19. Thus the effective melting temperature of unstretched sample was tentatively assumed to be 0 °C. The value of α_e was assumed to be 2.2 on the basis of the experimental data in the previous study.[20] Finally, eq 9 was assumed to hold also for the nonequilibrium melting behavior because it describes the increase in melting temperature due to the stretching. Then, from eq 9, we obtain

$$\nu = \frac{2\Delta H}{k\left(\alpha^2 + \frac{2}{\alpha} - 3\right)}\left(\frac{1}{T_m(1)} - \frac{1}{T_m(\alpha)}\right) \tag{20}$$

By assuming $\alpha = 2.2$ ($= \alpha_e$), $T_m(1) = 273$K and $T_m(\alpha) = 298$ K, the value of ν_0 was estimated to be 1.6×10^{-3} mol/cm^3 for NR from eq 20. According to eq 11, the value of ϕ is calculated to be $\bar{\nu}/\nu_0$, which distributes between 0.063 and 0.13 for the NR samples in Table 1. Because the assumptions for the above estimation of ν_0 and ϕ values are still not fully justified, we may have to find a more rigorous method for the future study.

It is noted that James and Guth[35] did not mention the viscoelastic contribution of the fluid-like component. Because their primary concern was the equilibrium behavior of rubber elasticity, the time-dependent response was excluded from their theory. They considered that the major effect of the fluid-like component was the internal pressure in bulk rubber.[35] However, the different behaviors between NR and IR samples in Figure 8 indicate that the fluid-like component also affects the time-dependent mechanical response of the rubber material. This kind of viscoelastic behavior will influence, for example, the grip performance or the energy consumption of pneumatic tires. Thus, analysis of the rubber material considering the composition of the elastically effective and the fluid-like components could open a new window for further development of high-performance products not only through the use of strain-induced crystallization behavior but also by controlling the viscoelastic behavior.

Conclusion

By assuming the cross-linked rubber to be composed of the elastically effective component and the fluid-like one, we could explain the features of strain-induced crystallization in the consistent manner with the formulations on the basis of the statistical theory. The experimental results for the series of cross-linked NR samples suggested that they happened to have a common ν_0 value for the elastically effective component, though their apparent network-chain densities were different from each other. As the model has suggested, the normalized stress−strain curves of the IR samples overlapped well with each other, as long as the extension ratio was low. The discrepancy observed for the NR samples was interpreted as the viscoelastic contribution of the fluid-like component containing the nonrubber contents. In this way, a route to understand the features of strain-induced crystallization along with the tensile properties of cross-linked NR and IR samples was presented through minimum increases in the number of parameters. This treatment should be valid mostly before the onset of strain-induced crystallization; we still have to explore a proper model to describe the tensile and strain-induced crystallization behavior of the crystallized rubber.

Acknowledgment. The author is grateful to Prof. S. Kohjiya, Mahidol University, and Dr. S. Toki, State University of New York at Stony Brook, for many helpful discussions, to Prof. Y. Ikeda, Kyoto Institute of Technology, Dr. S. Poompradub, Chulalongkorn University, Dr. K. Senoo, Sumitomo Bakelite Co., Ltd., and Prof. B. S. Hsiao, State University of New York at Stony Brook, for sample preparation and experimental help, to Prof. M. Tsuji, Kyoto University, for correction of the manuscript. This study was partly supported by a Grant-in Aid for Scientific Research (C), No. 20550187 from Japan Society for the Promotion of Science.

References and Notes

(1) Allen, P. W.; Jones, K. P. In *Natural Rubber Science and Technology*; Roberts, A. D., Ed.; Oxford University Press: Oxford, U.K., 1988; pp 1−34.
(2) Gent, A. N.; Kawahara, S.; Zhao, J. *Rubber Chem. Technol.* **1998**, *71*, 668–678.
(3) Trabelsi, S.; Albouy, P.-A.; Rault, J. *Macromolecules* **2002**, *35*, 10054–10061.
(4) Tosaka, M.; Kawakami, D.; Senoo, K.; Kohjiya, S.; Ikeda, Y.; Toki, S.; Hsiao, B. S. *Macromolecules* **2006**, *39*, 5100–5105.
(5) Tosaka, M. *Polym. J.* **2007**, *39*, 1207–1220.
(6) Mandelkern, L. *Rubber Chem. Technol.* **1993**, *66*, G61–G75.
(7) Gent, A. N. *Trans. Inst. Rubber Ind.* **1954**, *30*, 139–143.
(8) Kawahara, S.; Nishiyama, N.; Kakubo, T.; Tanaka, Y. *Rubber Chem. Technol.* **1996**, *69*, 600–607.
(9) Nishiyama, N.; Kawahara, S.; Kakubo, T.; Hwee, E. A.; Tanaka, Y. *Rubber Chem. Technol.* **1996**, *69*, 608–614.
(10) Kawahara, S.; Kakubo, T.; Sakdapipanich, J. T.; Isono, Y.; Tanaka, Y. *Polymer* **2000**, *41*, 7483–7488.
(11) Burfield, D. R. *Polymer* **1984**, *25*, 1823–1826.
(12) Kohjiya, S.; Tosaka, M.; Furutani, M.; Ikeda, Y.; Toki, S.; Hsiao, B. S. *Polymer* **2007**, *48*, 3801–3808.
(13) Treloar, L. R. G. *The Physics of Rubber Elasticity*, 3rd ed.; Clarendon Press: Oxford, U.K., 1975.
(14) Katz, J. R. *Naturwissenschaften* **1925**, *19*, 410–416.
(15) Clark, G. L.; LeTourneau, R. L.; Ball, J. M. *Rubber Chem. Technol.* **1941**, *14*, 546–554.
(16) Mitchell, G. R. *Polymer* **1984**, *25*, 1562–1572.
(17) Murakami, S.; Senoo, K.; Toki, S.; Kohjiya, S. *Polymer* **2002**, *43*, 2117–2120.
(18) Toki, S.; Sics, I.; Ran, S.; Liu, L.; Hsiao, B. S.; Murakami, S.; Senoo, K.; Kohjiya, S. *Macromolecules* **2002**, *35*, 6578–6584.
(19) Tosaka, M.; Kohjiya, S.; Murakami, S.; Poompradub, S.; Ikeda, Y.; Toki, S.; Sics, I.; Hsiao, B. S. *Rubber Chem. Technol.* **2004**, *77*, 711–723.
(20) Tosaka, M.; Murakami, S.; Poompradub, S.; Kohjiya, S.; Ikeda, Y.; Toki, S.; Sics, I.; Hsiao, B. S. *Macromolecules* **2004**, *37*, 3299–3309.
(21) Everaers, R.; Kremer, K. *J. Mol. Model.* **1996**, *2*, 293–299.
(22) Everaers, R. *New J. Phys.* **1999**, *1*, 12.1–12.54.
(23) Luch, D.; Yeh, G. S. Y. *J. Macromol. Sci., Phys.* **1973**, *B7*, 121–155.
(24) Luch, D.; Yeh, G. S. Y. *J. Polym. Sci., Polym. Phys.* **1973**, *11*, 467–486.
(25) Valladares, D.; Yalcin, B.; Cakmak, M. *Macromolecules* **2005**, *38*, 9229–9242.
(26) Walters, M. H. *J. Polym. Sci., Part A* **1963**, *1*, 3091–3103.
(27) Göritz, D. *Angew. Makromol. Chem.* **1992**, *202/203*, 309–329.
(28) Reichert, W. F.; Göritz, D.; Duschl, E. J. *Polymer* **1993**, *34*, 1216–1221.
(29) Göritz, D.; Sommer, J.-U.; Duschl, E. J. *Kautsch. Gummi Kunstst.* **1994**, *47*, 170–174.
(30) Watabe, H.; Komura, M.; Nakajima, K.; Nishi, T. *Jpn. J. Appl. Phys.* **2005**, *44*, 5393–5396.
(31) Smith, K. J.Jr.; Greene, A.; Ciferri, A. *Kolloid-Z.* **1964**, *194*, 49–67.
(32) Poompradub, S.; Tosaka, M.; Kohjiya, S.; Ikeda, Y.; Toki, S.; Sics, I.; Hsiao, B. S. *J. Appl. Phys.* **2005**, *97*, 103529/1–103529/9.
(33) Trabelsi, S.; Albouy, P.-A.; Rault, J. *Macromolecules* **2003**, *36*, 7624–7639.
(34) Chenal, J.-M.; Chazeau, L.; Guy, L.; Bomal, Y.; Gauthier, C. *Polymer* **2007**, *48*, 1042–1046.
(35) James, H. M.; Guth, E. *J. Chem. Phys.* **1943**, *11*, 455–481.
(36) Yamamoto, M.; White, J. L. *J. Polym. Sci., Part A-2* **1971**, *9*, 1399–1415.
(37) Flory, P. J. *J. Chem. Phys.* **1947**, *15*, 397–408.
(38) Trabelsi, S.; Albouy, P.-A.; Rault, J. *Rubber Chem. Technol.* **2004**, *77*, 303–316.
(39) Burfield, D. R.; Tanaka, Y. *Polymer* **1987**, *28*, 907–910.
(40) Tanaka, Y. *Rubber Chem. Technol.* **2001**, *74*, 355–375.
(41) Ikeda, Y.; Yasuda, Y.; Makino, S.; Yamamoto, S.; Tosaka, M.; Senoo, K.; Kohjiya, S. *Polymer* **2007**, *48*, 1171–1175.

(42) Ikeda, Y.; Yasuda, Y.; Hijikata, K.; Tosaka, M.; Kohjiya, S. *Macromolecules* **2008**, *41*, 5876–5884.
(43) Miyamoto, Y.; Yamao, H.; Sekimoto, K. *Macromolecules* **2003**, *36*, 6462–6471.
(44) Toki, S.; Sics, I.; Ran, S.; Liu, L.; Hsiao, B. S.; Murakami, S.; Tosaka, M.; Kohjiya, S.; Poompradub, S.; Ikeda, Y.; Tsou, A. H. *Rubber Chem. Technol.* **2004**, *77*, 317–335.
(45) Toki, S.; Fujimaki, T.; Okuyama, M. *Polymer* **2000**, *41*, 5423–5429.
(46) Toki, S.; Sics, I.; Hsiao, B. S.; Tosaka, M.; Poompradub, S.; Ikeda, Y.; Kohjiya, S. *Macromolecules* **2005**, *38*, 7064–7073.
(47) Toki, S.; Hsiao, B. S.; Kohjiya, S.; Tosaka, M.; Tsou, A. H.; Datta, S. *Rubber Chem. Technol.* **2006**, *79*, 460–488.
(48) Tosaka, M.; Senoo, K.; Kohjiya, S.; Ikeda, Y. *J. Appl. Phys.* **2007**, *101*, 84909.
(49) Ikeda, Y.; Higashitani, N.; Hijikata, K.; Kokubo, Y.; Morita, Y.; Shibayama, M.; Osaka, N.; Suzuki, T.; Endo, H.; Kohjiya, S. *Macromolecules* **2009**, *42*, 2741–2748.
(50) Gregg, J. E.; Macey, J. *Rubber Chem. Technol.* **1973**, 47−66.
(51) Karino, T.; Ikeda, Y.; Yasuda, Y.; Kohjiy, S.; Shibayama, M. *Biomacromolecules* **2007**, *8*, 693–699.
(52) Toki, S.; Burger, C.; Hsiao, B. S.; Amnuaypornsri, S.; Sakdapipanich, J.; Tanaka, Y. *J. Polym. Sci., Part B: Polym. Phys.* **2008**, *46*, 2456–2464.
(53) Toki, S.; S.; Hsiao, B.; Amnuaypornsri, S.; Sakdapipanich, J. *Polymer* **2009**, *50*, 2142–2148.
(54) Kawamura, T.; Urayama, K.; Kohjiya, S. *Macromolecules* **2001**, *34*, 8252–8260.
(55) Urayama, K.; Kawamura, T.; Kohjiya, S. *Macromolecules* **2001**, *34*, 8261–8269.
(56) Bekkedahl, N.; Wood, L. A. *Ind. Eng. Chem.* **1941**, *33*, 381–384.
(57) Kawahara, S.; Takano, K.; Yunyongwattanakorn, J.; Isono, Y.; Hikosaka, M.; Sakdapipanich, J. T.; Tanaka, Y. *Polym. J.* **2004**, *36*, 361–367.
(58) Armistead, K.; Goldbeck-Wood, G.; Keller, A. *Adv. Polym. Sci.* **1992**, *100*, 221–312.
(59) Dalal, E. N.; Taylor, K. D.; Philips, P. J. *Polymer* **1983**, *24*, 1623–1630.
(60) Kim, H.-G.; Mandelkern, L. *J. Polym. Sci. A-2* **1972**, *10*, 1125–1133.
(61) Edwards, B. C. *J. Polym. Sci., Polym. Phys. Ed.* **1975**, *13*, 1387–405.